ELSEVIER

Chemical Geology 146 (1998) 65–85

CHEMICAL GEOLOGY
INCLUDING
ISOTOPE GEOSCIENCE

Electron microprobe dating of monazites from high-grade gneisses and pegmatites of the Kerala Khondalite Belt, southern India

Ingo Braun *, Jean-Marc Montel, Christian Nicollet

Département de Géologie, Université Blaise Pascal, 5, Rue Kessler, F-63038 Clermont-Ferrand, France

Received 25 August 1996; accepted 21 November 1997

Abstract

Monazites of five samples (one leptynitic garnet–biotite gneiss, one khondalite, one augen gneiss and two pegmatites) from the central and northern part (Ponmudi Unit) of the Kerala Khondalite Belt (KKB) in southern India were analyzed with the electron microprobe dating technique. Monazites in the augen gneiss and the pegmatites yield grain sizes between 200–800 μm, Th abundances are rather low (<10 wt.%) and the distribution of Th, U and Pb within single grains is fairly homogeneous. Contrasting to this, monazites in the leptynitic gneiss and the khondalite are small (<150 μm). They often display very complex Th–U–Pb patterns and contain high Th concentrations up to 20 wt.%. The statistical treatment of individual ages from the investigated samples revealed three populations of Lower Proterozoic (~ 1.9 Ga), Upper Proterozoic (~ 580 Ma) and Ordovician age (~ 470 Ma) as well as Mid Proterozoic ages between 0.8–1.7 Ga which are not regarded to be of geological significance. Lower Proterozoic ages are preserved in the cores of monazites from leptynitic gneisses and khondalites. They fairly agree with Sm–Nd model ages for similar rocks of the KKB and give a minimum age for first monazite growth or complete homogenization. The prominent Pan-African population with mean values between 540 and 580 Ma is present in the leptynitic gneiss, the khondalite and the augen gneiss and in line with published isotope ages for the KKB. The Ordovician population finally marks the emplacement of granitic pegmatites subsequent to the Pan-African high-grade metamorphic event. There is an obvious discrepancy between khondalites and leptynitic gneisses on the one hand and augen gneisses on the other concerning the presence of Lower Proterozoic ages. While these are abundant in the former, often rimmed by Upper Proterozoic ages, they are completely absent in the latter. It appears unlikely that Lower Proterozoic ages were completely reset during a Pan-African event exclusively in the augen gneisses while they were preserved in leptynitic gneisses and khondalites. It is further concluded that the augen gneisses are of magmatic origin and were derived from porphyritic granites. Thus, the Upper Proterozoic age of 605 ± 37 Ma calculated for the investigated sample approximates the time of magma emplacement, which slightly precedes the peak stage of Pan-African high-grade metamorphism in the KKB, and of monazite crystallization from the granitic melt. A characteristic feature of the investigated monazites is the resetting of Lower Proterozoic and Pan-African ages to significantly younger values due to partial Pb loss. Monazites not shielded by other minerals (e.g., garnet) suffered selective mobilization of Pb along fractures or at their rims while Th and U concentrations remained almost unchanged. The results presented in this study indicate that

* Corresponding author. Mineralogisch-Petrologisches Institut, Universität Bonn, Poppelsdorfer Schloß, D-53115 Bonn, Germany. E-mail: ingo.braun@uni-bonn.de.

PII S0009-2541(98)00005-9

this was mainly due to fluid-rock interaction. It is concluded that thermal diffusion of Pb even at the suggested temperatures of 900°C only had minor influence on the Th–U–Pb composition in monazite and that the closure temperature for this system must be significantly higher than previously assumed (~ 750°C).

Keywords: Kerala Khondalite Belt; Monazite; Age dating

1. Introduction

Dating of monazite with the electron microprobe has been successfully applied to magmatic and metamorphic rocks throughout the last years (Suzuki and Adachi, 1991, 1994; Suzuki et al., 1994; Montel et al., 1994, 1996; Rhede et al., 1996; Cocherie et al., 1997) and provides a fast and cheap alternative to other in-situ techniques like the ion-probe or laser ablation-ICP-MS. Like these electron microprobe dating allows to correlate the location of the measurement within the monazite (core or rim) and the petrographical position of the crystal within the rock (interstitial along grain boundaries or included in other phases) with the calculated age. The high spatial resolution of the microprobe (≤ 5 μm) further enables to carry out a large number of analyses and to detect age and compositional inhomogeneities or zonations even on a small scale (few microns) (Cocherie et al., 1997).

This method has two main disadvantages compared to the ion-probe or LA-ICP-MS. First, its precision and sensibility is one order of magnitude worse and the usual uncertainty lies between ± 20–± 50 Ma. Therefore, samples younger than ca. 100 Ma can rarely be dated. The second disadvantage is that it is still not possible to test the closed-system hypothesis because the Pb isotopic composition, which could provide information if the analyzed domain is discordant or concordant, remains unknown.

Thus, the main fields of investigation are: (1) Dating rocks of unknown age. Microprobe dating provides a first general and quick overview of the age and the preserved age populations which might form a basis for further and more detailed isotope investigations. (2) Investigation of compositional and age heterogeneities within individual monazite grains. Like zircon monazite can consist of domains that formed during different magmatic or metamorphic events and display a significant contrast in age and Th–U–Pb composition. Additionally, it has been shown that monazite easily interacts with hydrothermal fluids (Poitrasson et al., 1996; Teufel and Heinrich, 1997) which preferentially dissolve Pb and thus disturb the Th–U–Pb systematics seriously. Electron microprobe dating due to its high spatial resolution is able, better than other in-situ techniques, to distinguish different domains within a monazite very precisely and to characterize the process through which they formed.

This paper presents results of electron microprobe dating of monazites from granulite-facies migmatitic gneisses and from pegmatites of the Kerala Khondalite Belt (KKB) in southern India. Representative samples of major rock types (garnet-bearing metagreywackes, metapelites and granitic augen gneisses) from the central and northern part (Ponmudi Unit) of this high-grade terrane were investigated. The main objective of this study was, in addition to the set of already published isotope ages [1] (Choudhary et al., 1992; Harris et al., 1994; Brandon and Meen, 1995), to reveal the geochronological information preserved in the lithotypes that form the gneissic basement of the KKB (do they provide any information that could be related to the Nd and Sr model ages which range between 2 and 3 Ga? do all gneisses provide similar ages or age distribution pattern or are different pieces of information preserved which finally could contribute to a better understanding of the tectonometamorphic evolution of the KKB?). Another point of interest focused on the interaction between the monazites and hydrous fluid phases which apparently

[1] Buhl, D., 1987. U–Pb und Rb–Sr-Altersbestimmungen und Untersuchungen zum Strontiumisotopenaustausch an Granuliten Südindiens. Unpubl. PhD thesis, Universität Münster.

affected the gneisses during different stages of their post peak-metamorphic evolution and to which extent the Th–U–Pb systematics of the monazites was disturbed by this hydrothermal activity.

2. Geological setting

The Late Proterozoic Kerala Khondalite Belt (KKB) south of the Achankovil Shear Zone (ASZ) (Fig. 1) forms the southernmost part of the Precambrian basement of India. Based on lithologic, petrologic and geochronologic criteria, it is suggested that, at least during the Late Precambrian, the KKB together with southern Madagascar and Sri Lanka formed part of the Mozambique Belt in the eastern part of Gondwana (Nicollet, 1990; Harris et al., 1994; Hölzl et al., 1991, 1994; Paquette et al., 1994; Windley et al., 1994).

The KKB is divided into two units with a discernible lithology. The Ponmudi Unit in the central and northern part is mainly composed of garnet biotite gneisses (leptynitic (*para*-)gneisses and granitic augen(*ortho*-)gneisses) and khondalites (grt–sil–bt(–crd)-paragneisses) as well as minor abundances of (arrested) charnockites, mafic granulites, calc-silicate rocks and cordierite gneisses. According to Chacko et al. (1992), the Ponmudi Unit represents a sequence of supracrustal rocks, whose protoliths in part probably were derived from massive charnockites of the Cardamom Hills Massif north of the ASZ (Fig. 1), and which were subjected to intense polyphase deformation and upper-amphibolite to granulite facies metamorphism during Pan-African orogeny $\sim$ 550 Ma ago.

The southern part of the KKB (Nagerkovil Unit) predominantly consists of garnet-bearing gneisses, charnockites and enderbites as well as of garnet-bearing mafic granulites which probably represent a highly deformed magmatic arc (Srikantappa et al., 1985). Supracrustal rocks are clearly less abundant than in the Ponmudi Unit.

Metamorphic P–T conditions inferred from charnockites and khondalites (Srikantappa et al., 1985; Chacko et al., 1987) yielded values of $\sim$ 750°C, $\sim$ 6 kbar and $a_{H_2O} \sim 0.3$. However, the results of two-feldspar thermometry (Fuhrman and Lindsley, 1988; Kroll et al., 1993) carried out on leptynitic garnet–biotite gneisses from the Ponmudi Unit indicate significantly higher temperatures of ca. 900°C (Braun et al., 1996) which recently were confirmed by the application of Al-in-opx-thermobarometry on KKB rocks by Chacko et al. (1996).

Nd and Sr model ages for gneisses and charnockites of the Ponmudi Unit range between 2.0 and 2.7 Ga (Choudhary et al., 1992; Köhler et al., 1993; Harris et al., 1994; Brandon and Meen, 1995) and are significantly lower for cordierite gneisses ($\sim$ 1.3 Ga; Brandon and Meen, 1995) which exclusively occur along the Achankovil Shear Zone.

Pan-African granulite facies metamorphism and subsequent arrested charnockite formation occurred about 550 Ma ago. Choudhary et al. (1992) reported a garnet/whole-rock Sm–Nd age of 558 Ma for an arrested charnockite sample from Ponmudi Unit, which is in line with a U–Pb monazite age of 552 Ma from the same locality. [1] Rb–Sr biotite–plagioclase ages of 440 ± 9 Ma and 458 ± 9 Ma, respectively, from two gneiss samples of the Ponmudi quarry are cooling ages and reflect the post-metamorphic uplift of the rocks (Choudhary et al., 1992).

Age data on pegmatites from the KKB are very rare. Biotite and muscovite K–Ar ages of four chrysoberyl-bearing pegmatites (Soman et al., 1982) range between 445 and 478 Ma and were interpreted as intrusion ages. Contrary to this, $^{207}Pb/^{204}Pb$–$^{206}Pb/^{204}Pb$ isochrons for fluorapatite and monazite from granites and pegmatites yielded significantly higher values of 509 ± 25 Ma (Berger and Braun, 1997) and 523 ± 32 Ma (Braun et al., 1995), respectively.

3. Analytical techniques

3.1. Monazite identification

Monazite and zircon were the main accessory phases in the investigated samples. The distinction between them in polished thin sections with optical microscopy is rather easy when grain sizes are large

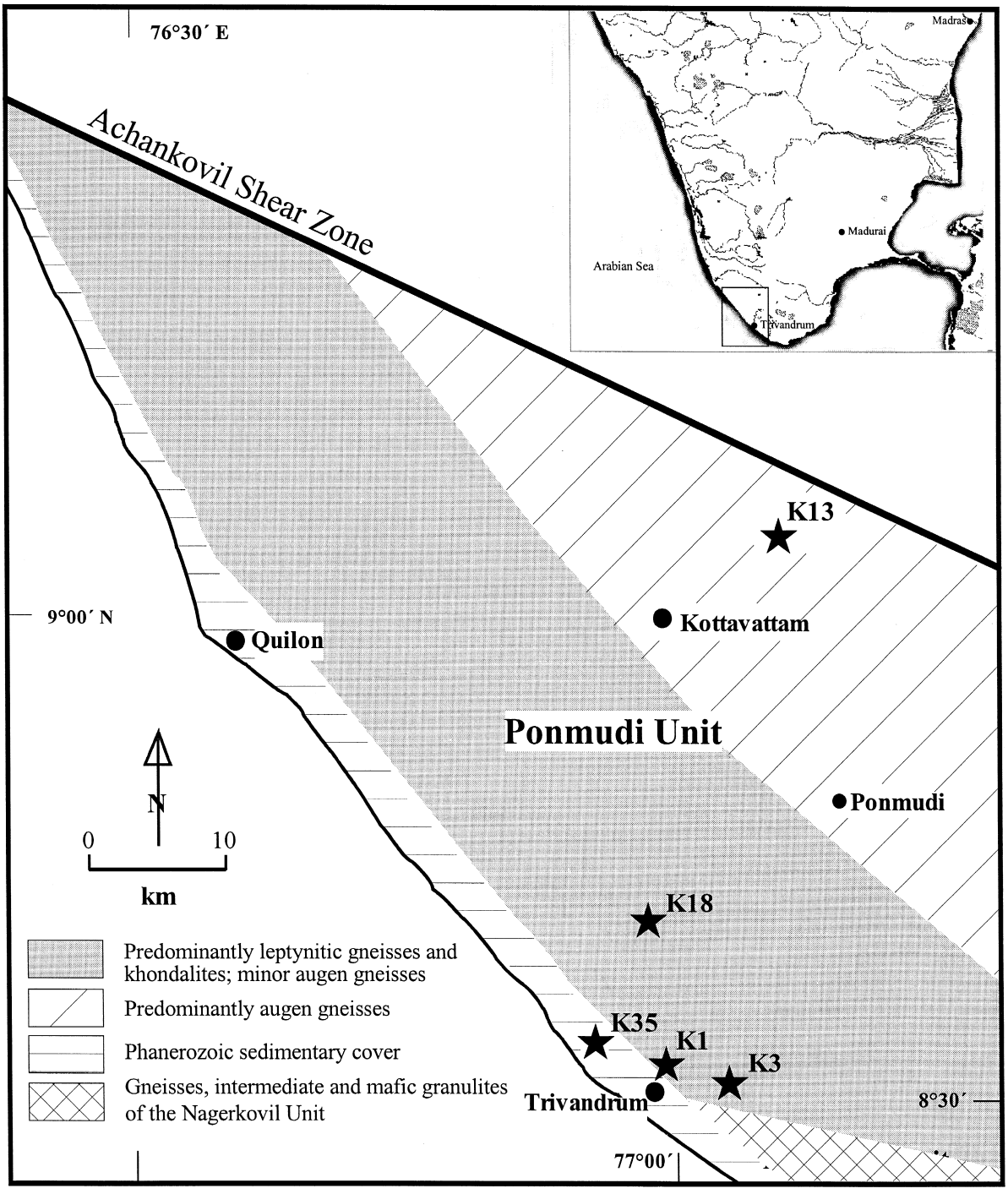

Fig. 1. Simplified map of southern India (inset) and the western part of the KKB. Sampling localities are indicated by stars.

and exceed 200 μm, which was the case only in the pegmatite samples. Here, monazite and zircon mostly could be distinguished by the following features: (a) The more or less distinct prismatic and euhedral shape of zircon, which contrasts with the predominantly rounded monazite grains. (b) The marked zoning of interference colors, which is characteristic of zircon but is absent or weakly expressed in monazite. (c) The occurrence and size of pleochroic halos. Those surrounding zircon were small and only found in biotite. In contrast, monazite, due to its high Th abundances (~ 10–20 wt.%), produced considerably larger halos in biotite and also cordierite. For the same reason, monazites were often surrounded by a halo in feldspar and garnet which was never recognized in the case of zircon.

In the gneiss samples, grain sizes rarely surpass 100 μm and mostly are about 50 μm in diameter. Consequently, the optical properties were difficult to determine properly and the distinction between zircon and monazite was not always successful. In such cases, the use of back-scattered electron images and scanning electron microscopy helped to identify even very small grains of monazite in the matrix or as tiny inclusions in garnet.

3.2. Microprobe work

U, Th and Pb were analyzed simultaneously on a CAMECA Camebax electron microprobe at the Département de Géologie, Université Blaise Pascal, Clermont-Ferrand. An accelerating voltage of 15 kV and probe currents of 80 to 140 nA were chosen as operating conditions. The counting times varied between 100 and 30 s (peak position). The U, Th and Pb concentrations were calculated using the ZAF correction procedure with an 'average' monazite composition for elements other than U, Th and Pb. For each measurement the statistical uncertainties are given at the 95% confidence level following the method of Ancey et al. (1978).

3.3. Age determination

Assuming that the abundance of common lead in monazite is negligible, which seems to be valid in most cases (Parrish, 1990), an age can be calculated for each data point when using the equation

$$\mathrm{Pb} = \frac{\mathrm{Th}}{232} \times \left(e^{\lambda^{232}t} - 1\right) \times 208 + \frac{\mathrm{U}}{238.04} \times 0.9928 \times \left(e^{\lambda^{238}t} - 1\right) \times 206 + \frac{\mathrm{U}}{238.04} \times 0.0072 \times \left(e^{\lambda^{235}t} - 1\right) \times 207$$

Since electron microprobe dating is a fast technique, processing time for one data point usually is less than 5 min which allows to obtain a large number (20–80) of rather imprecise ages (errors between 50 and 100 Ma) from a single thin section within a few hours. Therefore, a statistical procedure is necessary to (1) improve the precision by averaging the data, and (2) to check, on a firm mathematical basis, for the existence of a unique or multiple age populations. The method selected here is based on the least-squares concept because we want to compare a geological model with the data. For an age population obtained from a single sample (a thin section, usually) the most simple hypothesis is to assume that all analyzed domains were reset or formed at a time τ during an event that can be considered to have been instantaneous. The least-squares method then provides a best estimate of τ and a confidence interval $\pm 2\sigma_\tau$. It can now be estimated up to what extent the model is fulfilled by the data by calculating a numerical parameter, here the MSWD. Additionally, a statistical test, here the χ^2-test at the 5% confidence level, can be run to estimate if this agreement is acceptable or not. We must stress that like most statistical tests the χ^2-test yields a non-ambiguous answer only when it is negative (high MSWD) which means that we have to reject the model. A positive test in contrast (low MSWD) does not necessarily mean that the proposed model is correct; it just means that there is no statistical reason to reject it.

If the single age model is not acceptable another one has to be proposed. The most simple hypothesis in this case is that there are two geological events at times τ_1 and τ_2, each one having generated a population of domains. The procedure described in Montel et al. (1996) indicates how least-squares fitting is carried out in this case. If the two ages model is also

not acceptable, the procedure can be extended to three or more populations. In addition to a statistical test on the global model, expressed by a global MSWD, we also check the quality of each population that was identified by the procedure, using also a χ^2-test.

This statistical procedure provides a firm basis for discussing the results of electron microprobe dating of a sample but it has to be combined with other data for geological interpretation. These are:

– the age distribution as shown by the weighted-histogram representation,
– the geological relationships between the domains (core–rim relationships),
– the petrographical position of individual grains (interstitial, included in other minerals, along fractures),
– the composition-age relationships and
– the relative importance of each population.

4. Sample and monazite description

Fourteen samples (four leptynitic gneisses, three augen gneisses, one khondalite, six pegmatites), representing the main lithology of the Ponmudi Unit, were investigated. Out of these, five have been selected for presentation in this paper. Their mineralogical composition as well as their macro- and microtextural features are briefly described below. Additionally, the mode of occurrence, the shape and grain size of monazites in these rocks are given.

4.1. Leptynitic gneiss (K3)

Leptynitic gneisses in the KKB are fine- to medium-grained quartzofeldspathic rocks exhibiting a weak foliation which is defined by biotite. Accessory minerals are zircon, monazite, apatite and ilmenite. The characteristic textural feature of the leptynitic gneisses is the development of garnet-bearing in-situ leucosomes in a homogeneous biotite–quartz–feldspar matrix due to fluid-absent dehydration-melting at granulite facies conditions ($T \sim$ 900°C, $P > 6$ kbar, $a_{H_2O} \sim 0.3$; Braun et al., 1996).

Monazites are rare in the leptynitic gneisses. Only seven small grains ($\sim$ 30–100 μm in diameter) could be detected in the investigated thin section. They display a rounded or slightly oval shape and occur as inclusions in quartz, mesoperthitic alkalifeldspar and garnet. Most of them show a weak optical zonation (Fig. 2) in plane polarized light with a pale yellow core and a colorless rim.

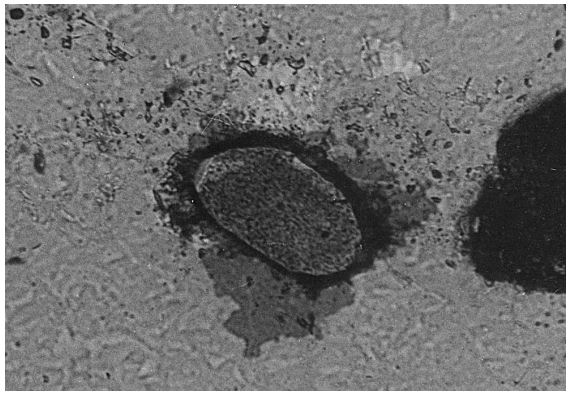

Fig. 2. Microphotograph of a monazite inclusion in quartz from the leptynitic gneiss sample K3 (see also Fig. 5a and b). Long side of the photograph is $\sim$ 300 μm.

4.2. Khondalite (K35)

Khondalites in the KKB are metapelitic rocks mainly composed of garnet, sillimanite, biotite, quartz, perthitic alkalifeldspar and/or plagioclase as well as accessory graphite, ilmenite, apatite, zircon and monazite. They were affected by intense ductile deformation during Pan-African orogeny and like the leptynitic gneisses experienced a strong migmatization which led to the development of garnet ($\pm$cordierite) bearing in-situ leucosomes. The retrograde metamorphic evolution followed a near-isothermal decompression path which is documented by cordierite–quartz rims around garnet. In the investigated thin section medium-grained garnet, which hardly contains any inclusions, occurs homogeneously distributed in the fine-grained biotite–sillimanite-rich gneiss matrix. The same section hosts a single poicilitic garnet porphyroblast with abundant inclusions of all other phases which is rimmed by cordierite–quartz symplectites.

Monazites exclusively appear as inclusions in the garnet poiciloblast and the associated cordierite–quartz rim. Their grain sizes hardly exceed 100 μm and their optical and morphological features are similar to those of monazites in the leptynitic gneisses.

Table 1
Calculated mean ages for the samples presented in this study

	Rock type	*N*	*t* (Ma)	±	*N*	*t* (Ma)	±	*N*	*t* (Ma)	±	*N*	*t* (Ma)	±	*N*	*t* (Ma)	±	MSWD
K1	p	26	474	22													1.32
K13	p	18	462	31													0.91
K18	ag	14	487	29	8	605	37										0.66
K3	lgn	19	482	22	16	585	23	9	1530	58	13	1966	58				1.57
K35	kh	30	542	23	8	832	62	4	1271	10	12	1713	76	13	1972	72	

lgn = leptynitic gneiss; kh = khondalite; ag = augengneiss; p = pegmatite; *N* denotes the number of analyses used for age calculation.

4.3. Granitic augen gneiss (K18)

This sample belongs to a group of garnet–biotite gneisses which predominantly occur toward the eastern part of the Ponmudi Unit. They are characterized by a conspicuous augen texture defined by the occurrence of cm-sized K–feldspar porphyroblasts in a rather fine- to medium-grained biotite–quartz–feldspar gneiss matrix. Garnet is a common mafic mineral which formed during migmatization of the gneisses and occurs homogeneously distributed and closely associated with biotite. Accessories are apatite, zircon, monazite and ilmenite which is often locally retrogressed and replaced by sphene. In contrast to the leptynitic gneisses accessory phases in the augen gneisses occur in higher modal abundances and yield significantly larger grain sizes.

Large grains (200–800 μm) of colorless monazite preferentially occur at the rims of K–feldspar porphyroblasts and form aggregates with biotite, plagioclase, ilmenite and zircon. They predominantly display subhedral shapes and slightly embayed grain boundaries and are almost free of inclusions. Although the sample provides evidence for an interaction of the rock with a hydrous fluid phase (retrogression of ilmenite and feldspars), the monazites themselves do not show any visible alteration, even when in close contact to retrogressed ilmenite.

Pegmatites of quartzmonzonitic (K1) and syenogranitic (K13) composition form small discordant dikes and veins in leptynitic gneisses and in augen gneisses. Field observations indicate that their emplacement postdates the ductile deformation and migmatization of the KKB gneisses during Pan-African Orogeny.

K1 was taken from a thin vein ($\sim$ 10 cm width) which cuts a leptynitic garnet–biotite gneiss discordant to its foliation. The sample consists of medium-grained biotite, plagioclase, quartz ± garnet, andalusite, ilmenite, monazite and zircon. Euhedral magmatic andalusite has been recognized in thin section and points to a crystallization of the melt at low pressure (< 4 kbar) and in the presence of a fluid phase rich in fluorine, chlorine or boron. [2]

K13 forms a dike of $\sim$ 20–30 cm width which occurs discordant in granitic augen gneisses. It is composed of coarse-grained quartz, potassic feldspar, plagioclase, garnet and pinitized cordierite and contains minor abundances of ilmenite, apatite, zircon and monazite.

Monazites in both samples have optical and morphological features that resemble those of the augen gneisses. The colorless grains yield sizes between 200 and 600 μm and occur interstitially between or included in quartz, feldspar and garnet. Like the augen gneiss, both pegmatites document hydrothermal activity which is reflected by retrogression of ilmenite (K13) or sericitisation of plagioclase (K1). Despite this, monazites in these samples appear fresh and do not seem to have participated in any exchange process with a fluid phase.

5. Results

5.1. General observations

The results carried out on 14 samples clearly demonstrate an apparent heterogeneity in Th–U–Pb

[2] Braun, I., 1997. Partielle Anatexis und Granitgenese unter granulitfaziellen Bedingungen: Der Kerala Khondalite Belt (Südindien) als Fallbeispiel. Unpubl. Ph.D. Thesis, University of Bonn, 179 pp.

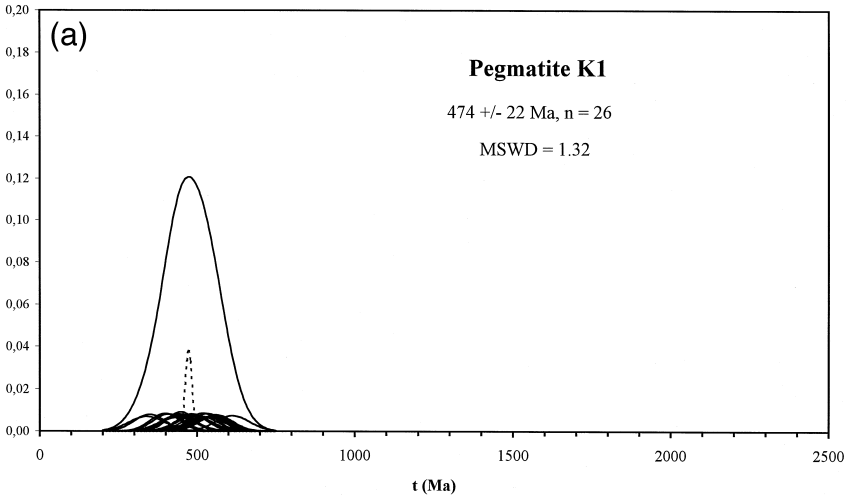
(a)
Pegmatite K1
474 +/- 22 Ma, n = 26
MSWD = 1.32
0,20
0,18
0,16
0,14
0,12
0,10
0,08
0,06
0,04
0,02
0,00
0
500
1000
1500
2000
2500
t (Ma)

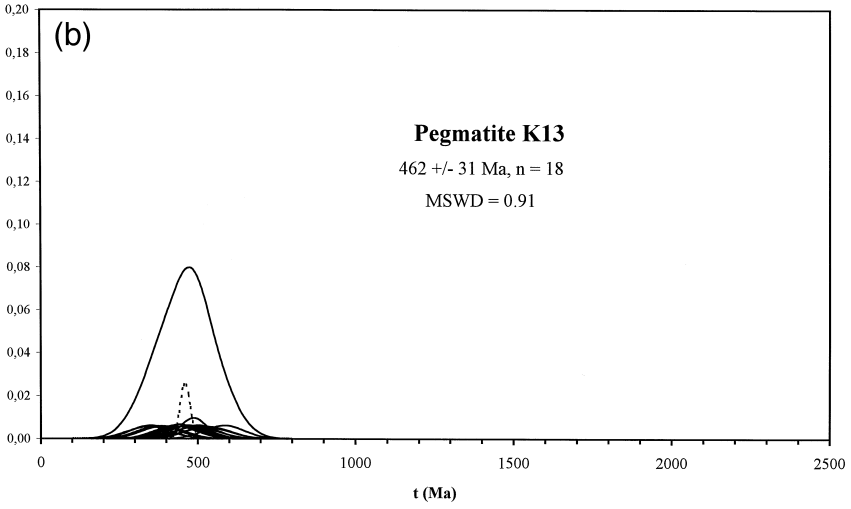
(b)
Pegmatite K13
462 +/- 31 Ma, n = 18
MSWD = 0.91
0,20
0,18
0,16
0,14
0,12
0,10
0,08
0,06
0,04
0,02
0,00
0
500
1000
1500
2000
2500
t (Ma)

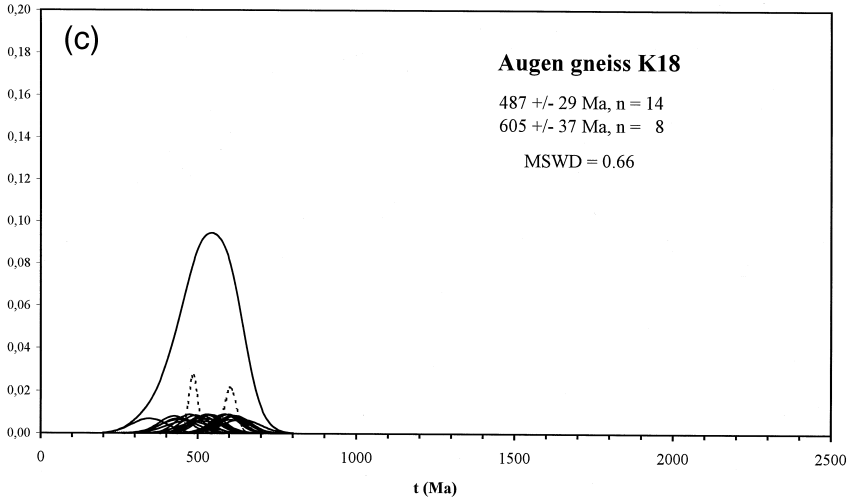
(c)
Augen gneiss K18
487 +/- 29 Ma, n = 14
605 +/- 37 Ma, n = 8
MSWD = 0.66
0,20
0,18
0,16
0,14
0,12
0,10
0,08
0,06
0,04
0,02
0,00
0
500
1000
1500
2000
2500
t (Ma)

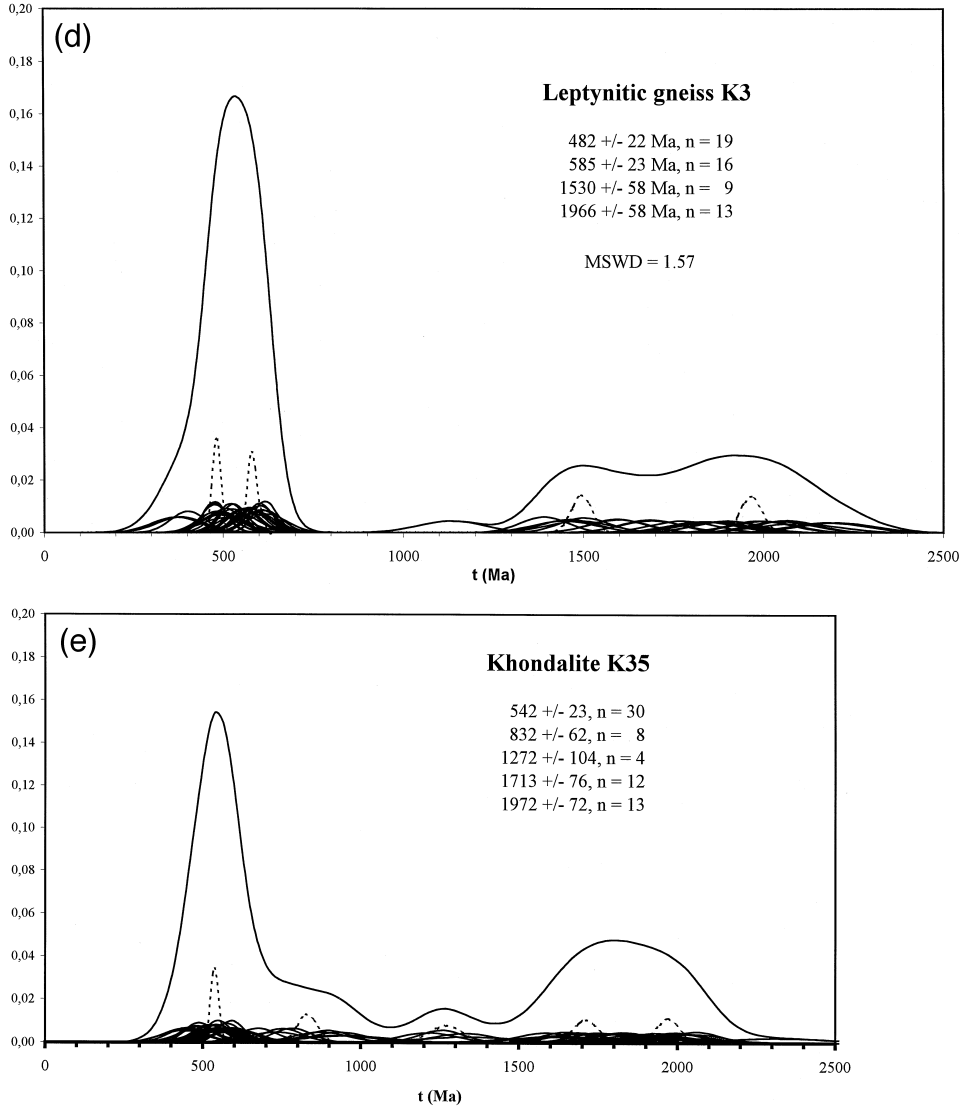

Fig. 3. (a–e) Weighted-histogram representations of the investigated samples. Shown are the bell-shaped curves for each measurement, the sum curve for all individual ages and the statistically derived age population(s) (dashed line(s)).

composition and in age distribution. Even single grains may display marked and complex zoning patterns with differences in Th concentration up to 10 wt.%. Monazites in leptynitic gneisses and khondalites show the highest Th (~ 22 and 15 wt.%), U (~ 2 and 3.8 wt.%) and Pb (~ 1.1 wt.%) abundances of all investigated rocks and yield the largest differences between minimum and maximum values. Contrary to this, monazites in augen gneisses and pegmatites display a more homogeneous Th–U–Pb composition and generally yield lower abundances (Th ≤ 10 wt.%; U ≤ 0.5 wt.%; Pb ≤ 0.3 wt.%).

This compositional difference between leptynitic gneisses and khondalites on the one hand and augen gneisses and pegmatites on the other finds its expression in the distribution of calculated ages. Whereas the former display a wide range and complex redistribution of ages from Lower Proterozoic (2.3 Ga) to

Pan-African (~550 Ma) and even younger values (~400 Ma), augen gneisses and pegmatites exclusively yield bimodal and unimodal Pan-African age populations, respectively (Table 1).

In Sections 5.2 and 5.3, each investigated sample will be discussed separately according to the scheme outlined in the section on age determination. We will first present the results for rocks with a simple uni- or bimodal age distribution (pegmatites and augen gneiss) and then turn to more complex cases with more than two age populations (khondalites, leptynitic gneisses). The appropriate data are shown in weighted-histogram representations (Fig. 3a–e) and U–Th-age diagrams (Fig. 4a–e) and are listed in Tables 2–6.

5.2. Simple age distributions

5.2.1. Quartz-monzonitic pegmatite (K1)

Six grains were investigated yielding a total of 26 analyses. Th concentrations range between 6.7–9.3

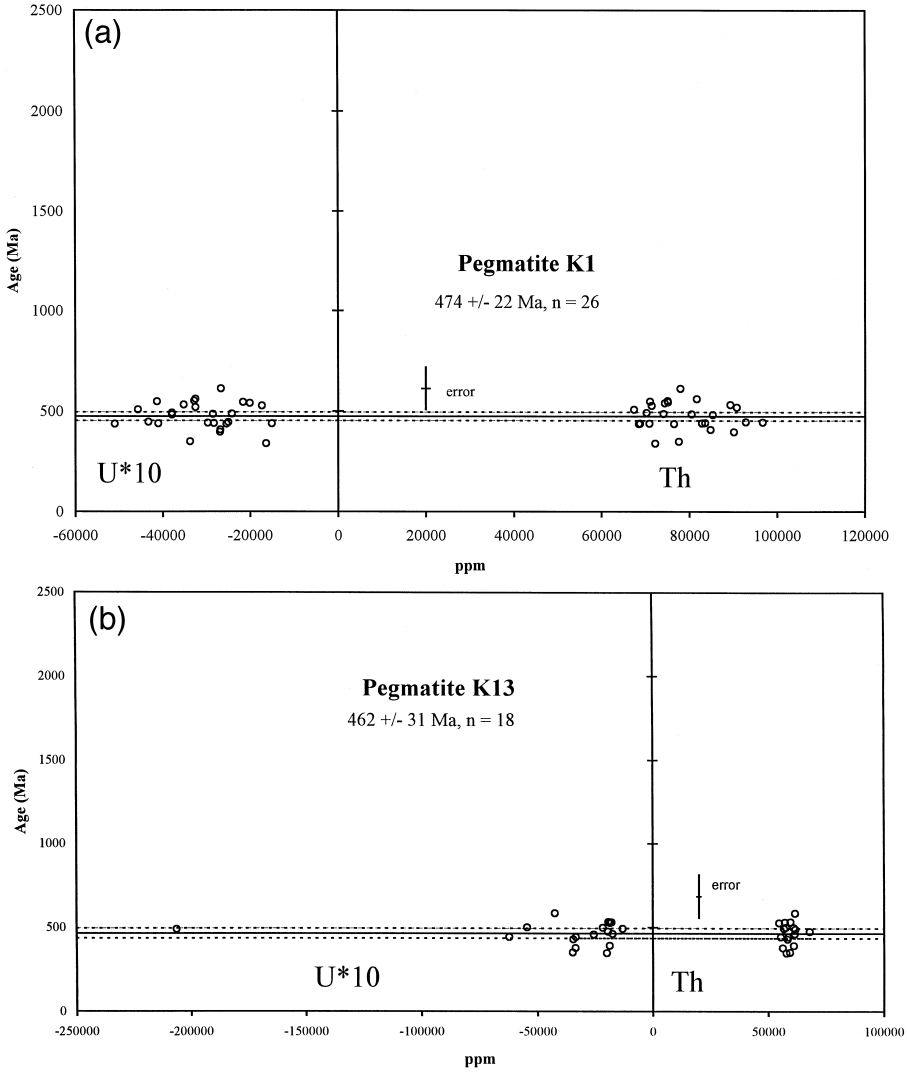

Fig. 4. (a–e) U–Th-age diagrams for the investigated samples displaying the relationship between individual ages, U (left side of the diagram) and Th content and their distribution around the calculated mean age for each population (solid line). Dashed lines represent standard deviations to each age population. For explanations see text.

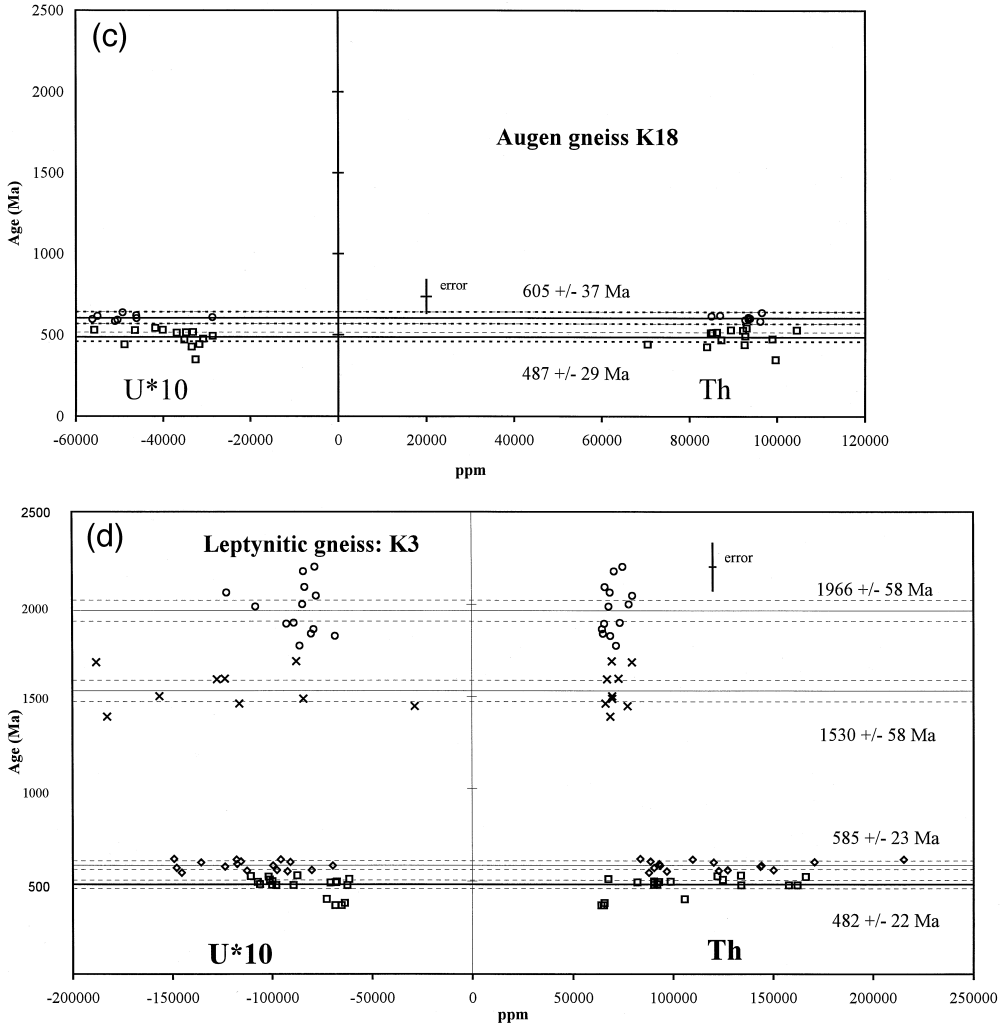

Fig. 4 (continued).

wt.%, U (0.15–0.51 wt.%) and Pb (0.12–0.24 wt.%) abundances are similar and significantly lower (Table 2).

Calculated ages range between 340 and 613 Ma and belong to a single population with a best estimate at 474 ± 22 Ma (MSWD = 1.32; Fig. 3a; Table 1). Fig. 4a shows that irrespective of the U or Th content all data points are arranged around the mean value of 474 Ma which indicates that there is no relationship between individual ages and the U and Th abundance in monazite. The calculated mean age is statistically not different from the $^{207}Pb/^{204}Pb$–$^{206}Pb/^{204}Pb$-isochron age on leachates from two monazite fractions of the same sample (523 ± 32 Ma; 4 points, MSWD = 0.08; Braun et al., 1995) and in good accordance with a $^{207}Pb/^{204}Pb$–$^{206}Pb/^{204}Pb$ apatite age of 509 ± 25 Ma from a fluorapatite–pegmatite, which is interpreted to approximate the time of melt emplacement (Berger and Braun, 1997).

5.2.2. Syenogranitic pegmatite (K13)

Eighteen measurements were made on five grains (Table 3). Th concentrations in this sample are highly uniform and range between 5.5 and 6.8 wt.%. U abundances range between 0.13 and 0.62 wt.% with

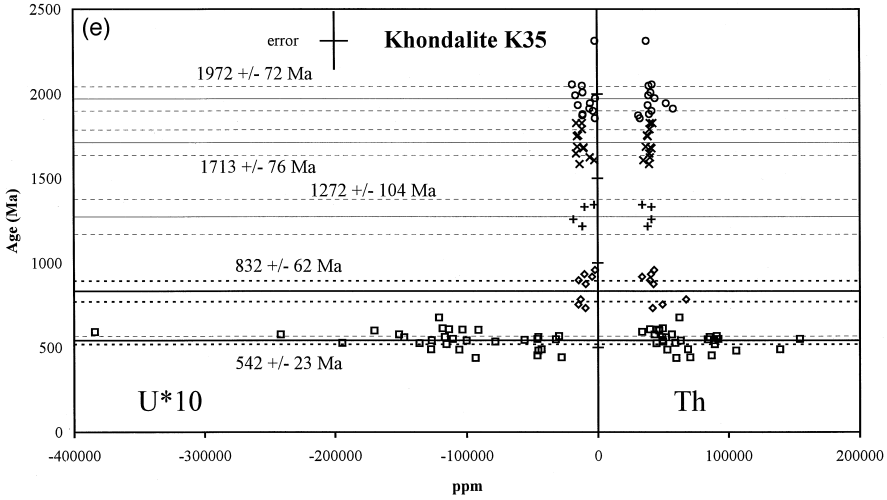

Fig. 4 (continued).

one exceptional high value of 2 wt.%. Pb abundances are rather low and vary between 0.10 and 0.28 wt.%.

Like in the pegmatite sample K1 the individual ages display a large scatter between 346 and 584 Ma (Table 3) but all belong to a single, unimodal population and are homogeneously distributed around the mean value of 462 ± 31 Ma (MSWD = 0.91) (Fig. 3b; Table 1). Again, the data do not provide any evidence for a relationship between individual ages and U and Th content (Fig. 4b).

The similar mean ages of the two investigated samples, which within error fit the values for other KKB pegmatites (Braun, unpubl. data), support the idea that monazite in these rocks was reset or formed during a Cambro–Ordovician event.

5.2.3. Augen gneiss (K18)

Seven monazite grains, one of them included in garnet, were analyzed and gave a total of 22 measurements (Table 4). Element concentrations are rather homogeneous (Th = 7–10 wt.%, U = 0.3–0.55 wt.%, Pb = 0.2–0.3 wt.%). Rarely, significantly lower Th and Pb values are observed at the contact to altered ilmenite.

The weighted-histogram representation for this sample suggests a similar unimodal age population as in the pegmatites. The statistical parameters, however, indicate that this model is not acceptable (MSWD = 3.46) and has to be rejected. Statistical treatment of the data assuming a bimodal age distribution yields two homogeneous populations at 487 $\pm$ 29 Ma (14 data points) and 605 ± 37 Ma (8 data points) and a global MSWD value of 0.66 (Table 1, Fig. 3c). The age-composition diagram (Fig. 4c) suggests that the two populations can be also distinguished by the U concentration which is systematically higher in the older population.

From this we conclude that the age data in this augen gneiss sample reflect two geochronological events. One is Ordovician in age and in agreement with the events identified in the pegmatites. The other is Upper Proterozoic in age and visible preferentially in monazite cores or in grains shielded by garnet which were not reset by the Ordovician pegmatitic event.

5.3. Complex age distributions

5.3.1. Leptynitic gneiss (K3)

Fifty-eight measurements were carried out on seven grains and yielded strongly varying U, Th and Pb concentrations (U = 0.3–1.9 wt.%, Th = 7–22 wt.%, Pb = 0.3–1.2 wt.%) (Table 5). The calculated ages range between 369 and 2203 Ma and define two clearly distinguishable age groups which are discussed separately hereafter.

Thirty-five measurements apparently define a unimodal Pan-African age population which is disproved by the statistical treatment of the data. In-

Table 2
Analytical results for monazites from the pegmatite sample K1

N		Th	±	U	±	Pb	±	t (Ma)	±
1	c	92,845	932	4321	400	2152	383	448	87
2	r	90,779	923	3246	392	2368	383	519	93
3	r	90,110	920	2683	394	1764	388	398	95
4	c	85,297	896	3784	397	2126	387	483	97
5	r	67,407	800	4563	400	1892	374	509	111
6	r	84,805	892	2681	391	1721	378	409	98
7	c	70,283	814	3783	395	1836	373	493	111
8	c	71,063	818	4125	402	2098	382	549	112
9	c_{fr}	72,194	828	1634	377	1183	370	340	114
10	r	74,375	837	2007	381	1973	376	540	115
11	r	75,136	842	2162	384	2022	379	545	114
12	r	71,445	820	1734	378	1833	375	528	120
13	r_{pl}	68,760	806	1505	381	1453	364	439	121
14	r_{pl}	77,606	852	3373	388	1390	368	349	100
15	c	74,129	835	2415	388	1803	378	488	113
16	r_{pl}	82,846	885	2825	392	1826	383	441	101
17	r	77,989	857	2663	389	2401	377	613	109
18	r_{pl}	76,535	848	2542	383	1670	369	437	106
19	r_{pl}	68,529	805	5099	408	1673	378	437	108
20	r	81,659	874	3249	388	2335	383	561	103
21	c	75,031	841	3276	390	2134	376	552	109
22	r_{pl}	83,591	888	2963	392	1856	386	442	101
23	r_{pl}	86,690	902	2496	388	1902	377	446	97
24	r_{pl}	80,532	869	2849	388	1963	374	486	102
25	r_{pl}	89,311	916	3515	394	2422	388	533	95
26	c_{fr}	70,879	817	4096	397	1670	374	440	108

Data for individual grains are separated by blank rows.
Counting time for each point was 100 s.
Subscripts 'fr' and 'pl' mark data points close to a fracture or sericitized plagioclase, respectively.

stead, a two-age model was calculated which consists of an Ordovician (482 ± 22 Ma, $n = 19$) and an Upper Proterozoic population (585 ± 23 Ma, $n = 16$). The 585 Ma age is regarded to reflect the Pan-African high-grade metamorphism and in fairly good agreement with the results of Buhl [1] (552 Ma, U–Pb isotope age of monazite) and Choudhary et al. (1992) (558 Ma, grt/whole rock Sm–Nd age). The 482 Ma age is identical to the ages reflected by the pegmatites. This distribution is very similar to the one found in the augen gneiss sample K18. Furthermore, the majority of ages belonging to the Upper Proterozoic population are characterized by higher U concentrations than the Ordovician ages which has also been recognized in the augen gneiss (Fig. 4d).

The Mid to Lower Proterozoic group is more heterogeneous. A three-age model with populations at 1456 ± 61 Ma ($n = 8$), 1804 ± 70 Ma ($n = 8$) and 2073 ± 81 Ma ($n = 7$) was calculated, but even in this case the population at 1456 Ma remains too heterogeneous to be statistically acceptable. It became obvious that the situation is much clearer if a single age of 1133 Ma is excluded. In this case, a four-age model for the remaining data set is acceptable (MSWD = 1.57) with, in addition to the Ordovician and the Upper Proterozoic group, a Mid Proterozoic (1530 ± 58 Ma, $n = 9$) and a Lower Proterozoic population (1966 ± 58 Ma, $n = 13$) (Fig. 3d). The age-composition diagram (Fig. 4d) shows that all populations have similar Th contents which

Table 3
Analytical results of the pegmatite sample K13

N		Th	±	U	±	Pb	±	t (Ma)	±
1	c	56,817	740	1307	373	1351	361	491	145
2	c	61,517	768	1732	380	1393	363	461	132
3	r_{ilm}	57,791	747	1993	382	997	366	346	136
4	c	57,228	745	1784	382	1501	364	529	142
5	r	61,285	766	2550	384	1432	367	457	128
6	c	54,796	730	1848	381	1439	362	526	147
7	r	61,107	768	1863	380	1175	364	390	131
8	c	59,632	758	1915	382	1582	366	532	137
9	c	67,944	805	1931	384	1587	371	474	122
10	r	61,703	770	20,635	517	2844	400	487	75
11	c	61,572	765	4240	403	1991	370	584	122
12	r	61,109	764	2151	383	1527	365	497	132
13	c	57,635	748	5446	409	1701	374	500	121
14	c_{fr}	58,741	752	6225	410	1574	373	442	114
15	c	55,498	737	3338	392	1320	370	442	135
16	r	58,434	752	3447	389	1344	372	429	129
17	c_{fr}	59,446	756	3480	390	1113	367	350	124
18	c_{fr}	56,261	740	3343	392	1134	367	376	131

Counting time for each point was 100 s.
Subscripts 'fr' and 'ilm' mark data points close to a fracture or retrogressed ilmenite, respectively.

Table 4
Analytical results for monazites of the augen gneiss sample K18

N		Th	±	U	±	Pb	±	*t* (Ma)	±
1	r	85,253	894	3474	396	2241	382	514	98
2	c	93,526	935	5620	410	3020	401	597	89
3	c	87,021	902	4620	408	2867	396	620	97
4	r_{ilm}	98,962	964	3081	395	2328	395	474	89
16	r_{ilm}	99,663	1443	3258	558	1709	522	346	114
17	r_{ilm}	92,596	1381	4883	569	2139	547	439	123
18	r	93,878	1391	4607	568	2971	542	603	125
19	r	96,580	1415	4931	575	3250	544	637	122
20	r	84,900	1312	3685	560	2237	542	512	138
21	r	104,456	1487	4003	569	2809	557	530	118
22	r	87,337	1337	3512	558	2080	541	468	134
5	r	93,082	933	4179	403	2606	394	541	91
6	r	92,749	933	5046	406	2923	400	592	91
7	r	93,461	935	2869	391	2824	394	608	96
8	r	86,313	901	3312	393	2251	386	515	98
9	c	85,033	892	5502	411	2875	390	617	95
10	c	92,758	933	2860	392	2264	387	493	93
11	r	84,030	890	3343	392	1816	381	425	98
12	r	96,201	950	5103	411	2985	400	585	88
13	c	89,475	916	5578	408	2576	389	530	89
14	r_{ilm}	70,484	816	3164	385	1601	368	441	111
15	c	92,232	930	4645	400	2553	394	527	90

Counting time for each point was 30 s.
Subscript 'ilm' marks analysis close to retrogressed ilmenite.

plot in a rather narrow range between 65,000–80,000 ppm (Table 5). Furthermore, the U concentrations for data points of the Lower Proterozoic group are also rather homogeneous which is in obvious contrast to the largely scattering Mid Proterozoic population (Fig. 4d). This can be interpreted in two ways. Either new domains with a distinct composition (high U concentration) were formed during a Mid Proterozoic event which at the moment is questionable. Or, the apparently Mid Proterozoic domains were Lower Proterozoic in age and subsequently affected by a chemical exchange which caused a gain of U or a loss of Pb. The 1966 Ma age is similar to Nd model ages for garnet–biotite gneisses and khondalites from the KKB (Choudhary et al., 1992; Brandon and Meen, 1995) and can be interpreted to reflect the timing of a Lower Proterozoic event.

The redistribution of ages as well as Th, U and Pb abundances within a complexly-zoned monazite is discussed in the next paragraph.

Fig. 2 shows a microphotograph of a monazite inclusion in quartz which has been studied in great detail. A weak zoning is recognized and expressed by a shaded core region and a bright rim. A SEM image of the same monazite grain is presented in Fig. 5a. The core shows straight crystal faces and strongly embayed grain boundaries, suggesting a former euhedral shape followed by subsequent interaction with a melt phase. Twenty-six measurements were carried out on this grain and revealed a systematic zoning in Th–U–Pb concentration and in age. Fig. 5a shows the location of the data points and the Th abundances within the monazite which range between 6.5 and 8 wt.% in the core and are significantly higher in the rim (> 9 wt.%). Pb concentrations are inverse to this. They predominantly range between 0.7 and 1.1 wt.% and are distinctly lower in the rim where they do not exceed 0.45 wt.%. U abundances do not show any zoning or systematic redistribution. The calculated ages are shown in Fig. 5b. It becomes obvious that the observed optical and chemical zoning of this monazite coincides with a contrasting age distribution between core and rim. In the core, Proterozoic ages are preserved and show a large scatter between 1.1 and 2.2 Ga (Fig. 5b; Table 5), thus reflecting the two Mid and Lower Proterozoic age populations mentioned above and shown in Fig. 5a. There is no obvious systematic age redistribution within the core, e.g., decrease in age from its inner part toward the outer parts which might indicate that the younger ages, constituting the mid-Proterozoic age population are the result of a disturbance of the Th–U–Pb systematics and a partial Pb loss. The bright, Th-rich rim in contrast exclusively displays Pan-African ages (478–615 Ma).

5.3.2. Khondalite (K35)

Nineteen monazite grains, included in the garnet porphyroblast or in the surrounding cordierite–quartz symplectites, were analyzed, yielding a total of 67 analyses. The results are given in Fig. 3e, Fig. 4e and

Table 5
Results for monazites of the leptynitic gneiss sample K3

N		Th	±	U	±	Pb	±	t (Ma)	±	N		Th	±	U	±	Pb	±	t (Ma)	±
1	c	90,428	957	14,779	479	3584	476	571	83	53	r_p	68,686	1315	18,254	743	8540	645	1390	132
										54	c	64,654	1265	7894	622	8175	628	1866	193
2	c	162,176	1340	6238	421	3914	505	476	67	55	c	69,562	1324	8769	638	7959	629	1690	176
3	c	215,194	1609	1609	447	6872	669	616	66	56	c	65,888	1281	9251	635	8874	644	1895	184
										57	r	91,994	1597	10,606	652	2749	500	482	99
4	c	134,128	1193	1193	434	3496	471	476	70	58	r	90,433	1577	9994	640	2654	493	478	101
5	r	133,872	1191	8737	434	3872	487	529	73	59	r_p	69,660	1326	15,631	711	8725	635	1502	141
										60	c	67,622	1302	4534	589	4317	541	1133	179
6	c	170,635	1382	9100	440	5450	579	601	71										
7	r	120,173	1117	13,552	464	4490	520	603	77	14	c	79,602	1374	18,799	736	11,593	952	1685	164
										15	c	87,830	1463	14,530	687	3328	583	544	107
8	c	70,687	843	8408	426	10,555	907	2179	210	16	c	83,565	1415	14,907	694	3719	597	619	113
8b	c	78,141	1430	8461	628	10,303	688	2001	181										
9	r	96,696	995	9233	440	3168	466	552	89	17	r	144,146	2077	9949	639	4658	629	583	90
10	c	75,091	869	7833	428	10,915	934	2203	212	18	r	150,236	2140	9766	629	4600	627	559	87
11	c	77,283	884	2855	387	5830	608	1448	179	19	r	143,594	2072	12,357	662	4816	642	578	88
12	r	72,841	857	12,349	458	8691	781	1597	161	21	r	90,508	1577	7079	612	2506	499	490	111
13	r	88,703	952	11,571	456	3467	470	605	91	22	c	105,700	1763	7279	622	2339	513	402	98
20	c	66,077	1221	8343	619	9619	852	2095	231	23	c	166,357	2474	10,171	648	4694	544	521	71
38	r	90,357	1577	9984	652	2763	504	498	103	24	c	93,452	1614	6975	618	3060	501	582	111
39	r	66,302	1287	11,621	672	7264	609	1461	157	25	c	157,888	2380	9801	661	4072	550	476	74
40	r_p	67,175	1296	12,737	678	8355	633	1594	156	26	c	124,860	1990	10,114	651	3613	536	507	86
42	r_p	68,042	1306	10,793	657	10,118	679	1989	178	27	c	122,705	1965	11,260	665	4004	543	555	87
43	c	68,639	1312	12,243	676	11,154	694	2065	171	28	c	122,077	1955	11,077	659	3753	545	526	88
44	c	69,572	1335	8428	630	6849	634	1488	177	29	c	127,174	2017	8024	628	3860	537	558	90
45	c	65,193	1274	8029	626	8144	631	1841	191	31	r	82,142	1477	6810	614	2324	490	493	118
46	c	73,567	1373	8887	632	9464	660	1901	178	32	r	98,741	1679	6767	625	2695	497	495	104
47	c	79,840	1450	7773	634	10,474	683	2047	184	33	r	67,506	1308	6144	604	2008	484	509	138
48	c	71,777	1354	8605	632	8540	646	1775	179	34	c_{fr}	64,019	1256	6528	605	1416	472	370	135
49	r_p	68,790	1314	6829	611	8008	619	1829	191	35	c_{fr}	65,365	1280	6842	606	1452	482	369	134
50	r	92,880	1608	10,724	663	2853	509	494	100	36	c_{fr}	65,826	1284	6406	609	864	493	223	135
51	r	92,959	1608	11,749	668	3522	518	592	101	37	c_{fr}	65,627	1282	6367	607	1483	466	382	132
52	r	109,613	1811	11,788	670	4132	536	615	94										

Counting times were 30 and 100 s, respectively.
r_p = rim of proterozoic core.
Subscript 'fr' marks analysis close to a fracture.

in Table 6. Average Th concentrations range between 3 and 5 wt.%, and are rarely as high as 8–10 or even 15 wt.%. Regardless of this, marked variations up to 5 wt.% within single grains are present. Pb and U abundances range between 0.2–1.1 wt.% and 0.2–3.8 wt.%, respectively.

The distribution of ages in the khondalite is slightly different to that in the leptynitic gneiss sample (K3). Two major groups around 500 Ma and 1800 Ma with abundant intermediate ages are present. The statistical treatment of the data yields five populations: one of Upper Proterozoic age (542 ± 23 Ma, $n = 30$), a Mid Proterozoic (1713 ± 76 Ma, $n = 12$) and a Lower Proterozoic population (1972 ± 72 Ma, $n = 13$) as well as two minor populations with mean ages of 832 ± 62 Ma ($n = 8$) and 1271 ± 104 Ma ($n = 4$) (Fig. 3e, Table 1). The Upper Proterozoic age population is homogeneous and the calculated age is within error in good agreement with the ages found in the leptynitic gneiss (K3) and the augen gneiss (K18). In the composition-age diagram (Fig. 4e) the Upper Proterozoic population displays largely varying U and Th contents which do not show any relationship to the corresponding ages. All

Table 6
Results for monazites of the khondalite sample K35

N		Th	±	U	±	Pb	±	*t* (Ma)	±	*N*		Th	±	U	±	Pb	±	*t* (Ma)	±
1	r	49,722	973	11,834	621	2458	475	611	134	36	c	41,526	890	10,595	606	6242	571	1678	193
2	r	47,060	950	17,012	675	2794	492	598	119	37	c	40,941	884	10,878	610	7731	597	2010	199
3	c	52,167	998	14,750	651	2539	490	558	121										
										38	c	58,132	1057	5786	556	7119	591	1913	211
4	c	154,455	1916	4608	553	4195	522	549	79	39	c	41,778	896	3122	532	4736	529	1901	288
5	r	87,022	1325	4619	545	2081	479	453	116	40	c	39,756	873	16,250	659	7568	593	1649	160
6	c	139,421	1797	4293	563	3379	535	489	87	41	r	62,395	1096	12,085	625	3136	499	675	123
										42	c	42,148	899	16,108	661	8687	621	1829	163
7	r	89,460	1348	11,537	622	2980	496	519	98										
8	c	43,396	910	15,126	652	2430	478	576	127	43	c_{fr}	33,858	813	38,384	863	4303	519	591	80
9	r	68,945	1157	12,711	632	2430	493	488	110	44	c	49,473	970	14,840	646	3388	489	753	126
10	r	63,350	1107	10,011	605	2346	471	540	122	45	r	92,172	1376	11,056	619	3182	500	548	98
11	r	59,935	1075	9315	594	1779	474	438	128	46	c	83,986	1298	3216	536	2325	476	546	127
12	r	89,063	1347	12,654	633	3199	505	542	97	47	c	40,107	874	11,348	616	2127	455	606	147
13	c	40,004	873	11,715	616	6947	582	1792	189	48	r	67,607	1147	13,069	633	3963	536	783	123
14	c	37,669	849	1598	507	4790	523	2315	366	49	c	52,603	1004	5216	552	6557	579	1946	229
15	c	38,088	854	14,434	643	7454	586	1757	173	50	c	39,791	872	10,941	605	7077	580	1881	196
16	c	35,142	829	2365	512	3253	485	1609	316	51	c	44,067	913	1395	514	4547	531	1976	321
17	c	38,510	863	15,606	652	7807	603	1750	168										
18	c	31,501	791	11,146	610	6385	570	1873	210	52	r	85,504	1314	4535	551	2539	490	560	123
19	r	49,553	973	5584	556	1665	458	543	168	53	c	46,866	946	9104	591	2089	468	601	152
										54	c	105,789	1496	4556	557	2611	496	481	103
20	c	59,341	1069	19,448	694	2926	490	526	99										
21	c	56,494	1044	24,139	735	3547	499	576	92	55	c	41,331	893	18,380	688	6100	562	1257	140
22	r	53,260	1009	10,553	614	1926	460	486	129										
										56	c	34,164	815	2537	510	2661	484	1343	307
23	c	39,315	869	16,385	662	9445	641	1992	168	57	c_{fr}	39,895	876	14,569	645	3648	504	897	145
24	c	41,961	897	18,992	686	11,028	662	2057	154	58	r	32,647	799	1655	509	3354	500	1857	376
25	r	42,036	905	9324	599	2434	493	733	170										
26	c	37,095	847	15,195	650	7266	585	1689	169	59	c	33,809	812	4184	529	2005	472	918	254
27	c	40,377	878	11,591	619	7098	581	1828	190	60	c	43,119	909	2168	522	2199	490	957	255
28	c	38,867	860	14,491	644	8427	614	1934	177	61	r	40,838	883	10,210	602	3211	494	933	169
29	r	44,804	925	13,580	638	2119	452	525	125	62	r	39,489	870	13,499	638	6485	568	1586	173
30	r	45,157	926	10,312	611	2161	468	603	148										
31	r	49,293	971	11,648	613	2220	469	561	133	63	c	38,278	860	11,600	613	4391	524	1215	176
										64	c	39,408	865	11,351	614	7932	589	2049	196
32	c	40,316	878	5647	549	4576	537	1625	244	65	r	40,773	881	10,270	605	6121	559	1685	195
33	c_{fr}	50,091	973	7818	578	1825	466	534	152	66	c	70,688	1177	2772	526	1581	468	441	144
34	r	42,769	905	9279	591	2947	476	874	166	67	r	90,834	1358	2959	533	2564	475	565	120
35	c	41,118	887	9918	604	4656	533	1330	187										

Counting time for each point was 30 s.
Subscript 'fr' marks analysis close to a fracture.

other age populations are homogeneous at constant Th and U abundances. There is clear evidence for a Lower Proterozoic event with an age identical to the one obtained from the leptynitic gneiss (1966 ± 58 Ma). Then there exist several poorly defined Mid Proterozoic populations whose significances remain rather unclear. As discussed for the leptynitic gneiss ages belonging to these populations could have been formed by an incomplete resetting of Lower Proterozoic ages. This interpretation is supported by the fact

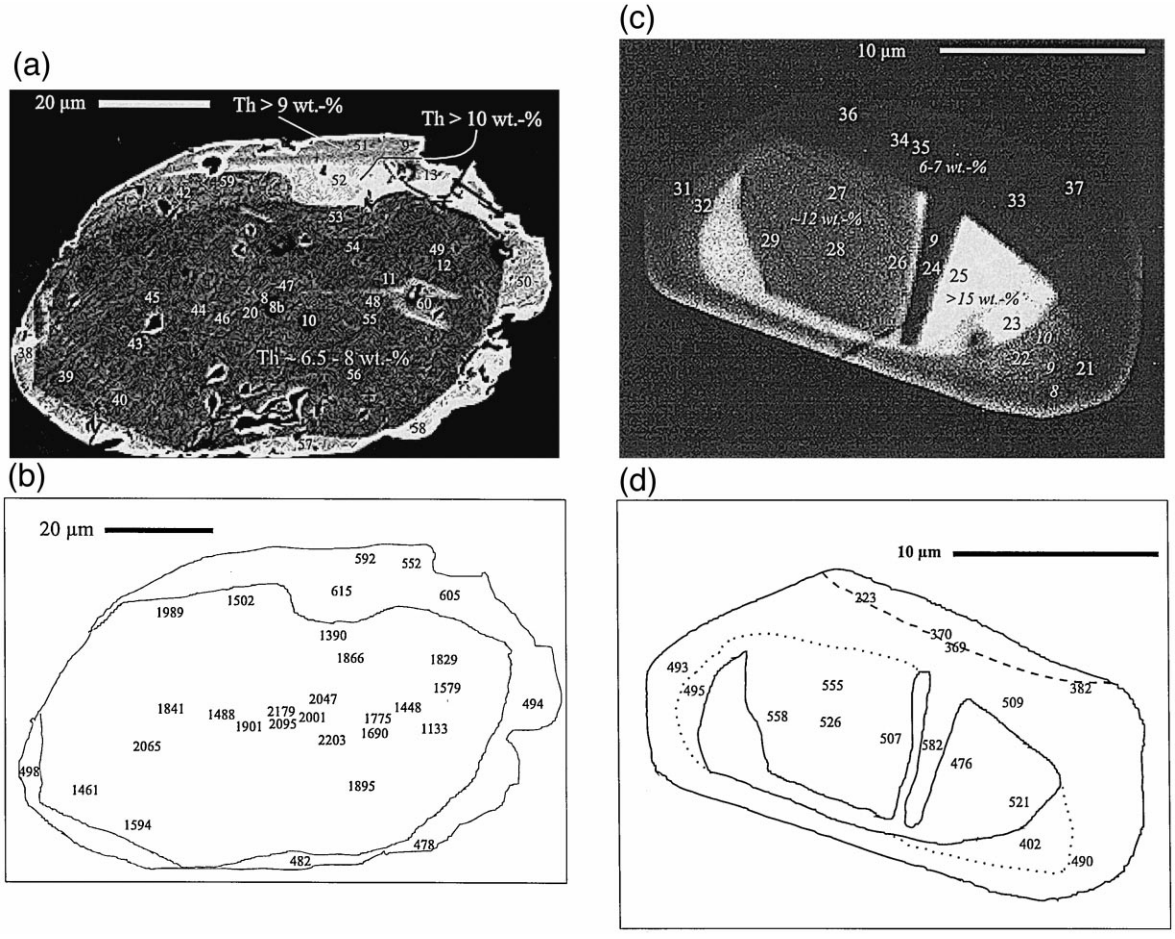

Fig. 5. (a–d) Monazites from the leptynitic gneiss sample K3. (a) SEM photograph of the monazite grain of Fig. 2 showing the zoned distribution of Th with low concentrations in the core and considerably higher values at the rim. Numbers refer to Table 5 and indicate the locations of measurements. (b) Sketch drawing of the same monazite grain with the calculated individual ages. The low-Th core exhibits largely varying Mid and Lower Proterozoic ages, while the Th-enriched rim exclusively shows Pan-African values. (c) The SEM image of a second monazite grain displays an extremely complex Th distribution pattern. (d) The corresponding ages, however, almost completely belong to a single Pan-African population. The strong age resetting along the fracture in the upper part of the monazite coincides with a marked depletion of Pb abundances (Th and U remain ±constant). It is suggested that resetting is due to selective Pb mobilization during fluid-rock interaction.

that we never unambiguously identified monazites of Mid Proterozoic age. In most cases these are systematically associated with a Lower Proterozoic core which preserved ages of ~2000 Ma and an Upper proterozoic, Pan-African domain of ~550 Ma at the outermost parts. The few grains with ages between 900–1500 Ma are always in contact with or transected by fractures, so that it cannot be ruled out that the obtained ages are artifacts and resulted from mobilisation of Pb due to interaction of the monazite with a circulating fluid phase.

One of the most striking points in this sample is the absence of an Ordovician population. Since all investigated monazites were included in cordierite and garnet it may be possible that the monazites were shielded by these minerals from being reset during the Ordovician pegmatitic event as it has been the case in the leptynitic gneiss and the augen gneiss.

6. Discussion

6.1. Geological implications

The results presented in this study clearly document at least three different stages of the tectonometamorphic evolution of the Kerala Khondalite Belt: a Lower Proterozoic stage at about 1970 Ma (present in the leptynitic gneiss and the khondalite), an Upper Proterozoic stage at ~580 Ma (in the gneisses) and an Ordovician stage at 470 Ma (all samples without the khondalite) (Table 1). The existence of Mid Proterozoic populations between 800 and 1700 Ma in the khondalite and the leptynitic gneiss sample is not well constrained and remains doubtful.

Lower Proterozoic ages are in fairly good agreement with Sm–Nd model ages of 2.0–2.7 Ga from garnet–biotite gneisses and khondalites (Choudhary et al., 1992; Brandon and Meen, 1995). We interpret them to reflect the time of first monazite growth which would provide an upper limit for the deposition of the sedimentary protoliths of leptynitic gneisses and khondalites. A close investigation of the location of the measurements that yielded Lower Proterozoic ages showed that they are predominantly preserved in the cores of monazites which occur as inclusions in quartz, garnet and cordierite but also along grain boundaries. The rims of these grains often display Upper Proterozoic ages which formed during Pan-African high-temperature metamorphism. This suggests that even temperatures of 900°C which were attained during this event did not result in a complete resetting of the Th–U–Pb systematics and left the cores more or less unaffected. Moreover it shows that shielding of monazites by their host minerals obviously played an effective role in preventing a complete resetting. It has to be taken into account that even the Lower Proterozoic ages which constitute the 1.9 Ga population may have resulted from resetting of ages >2 Ga. Thus they should be regarded as minimum values.

The most prominent population in the gneiss samples yields Upper Proterozoic values and mean ages range between 542 and 605 Ma (Table 1). These values are broadly in line with U–Pb, Rb–Sr and Sm–Nd isotope data carried out on similar rocks [1] (Choudhary et al., 1992; Köhler et al., 1993; Harris et al., 1994; Brandon and Meen, 1995) and reflect a prominent stage of monazite growth or recrystallization during Pan-African high-grade metamorphism.

The bimodal distribution of Lower Proterozoic and Pan-African ages in leptynitic gneisses and khondalites of the KKB is identical to what was recognized in similar rocks from southern Madagascar (Nicollet et al., 1995). Monazite grains from metapelite and charnockite samples which were collected inside the Precambrian basement and in shear zones also revealed a strong and irregular zoning of Th–U–Pb abundances and in some grains the preservation of Lower Proterozoic ages (~1.8 Ga) which are rimmed by Pan-African ages of ~550 Ma. In addition to the conformities between the two terranes regarding major tectonic elements (e.g., the Achankovil Shear Zone in the KBB, which is considered as the prolongation of the Bongolava–Ranotsara Shear Zone in southern Madagascar) and the lithology, these similarities provide further support for their common tectonometamorphic evolution during the Proterozoic.

Our investigation of the different gneisses forming the basement of the KKB revealed that augen gneisses in contrast to leptynitic gneisses and khondalites never yielded Lower or even Mid Proterozoic ages. This can be due to following reasons: (1) the number of analyzed samples was too low to be representative for the whole region; (2) Lower Proterozoic ages were present as in the other gneisses but were completely reset during the Pan-African event; (3) monazites in these rocks exclusively formed during the Upper Proterozoic and the calculated ages give the time of crystallization. Monazites in the augen gneisses generally are more abundant and yield larger grain sizes (200–800 μm) than in the leptynitic gneisses and the khondalites (<100 μm). Thus, if they all expected the same high-temperature overprint during Pan-African orogeny it should be expected that the large monazites in the augen gneisses were more suitable to preserve Lower Proterozoic than the rather small ones in the other gneisses and it appears difficult to explain why any pre-Pan African information was wiped out exclusively in the augen gneisses. Although there is undoubtedly a need that more samples have to be investigated to confirm or to disprove our results we

conclude that the absence of Mid or Lower Proterozoic ages in the investigated augen gneiss as well as in other similar rocks from the KKB (Braun, unpubl. data) is due to their magmatic origin. In accordance with the conspicuous augen texture of these rocks we propose that the precursor rocks were porphyritic granites which most likely intruded the basement of the KKB prior to the main phase of deformation. The calculated mean age for sample K18 (605 ± 37 Ma) which is slightly higher than for leptynitic gneisses and khondalites might indicate that granite emplacement occurred before the thermal peak of Pan-African high-grade metamorphism.

The age data carried out on monazites from K1 and K13 and other pegmatite samples (Braun, unpubl. data) range between 462 and 512 Ma. Within error they correspond to Pb–Pb isotope ages of monazites from sample K1 (523 ± 32 Ma; Braun et al., 1995) and apatites from another pegmatite sample (509 ± 25 Ma; Berger and Braun, 1997) and constrain a stage of late (final?) magmatic activity in the KKB which clearly postdates the peak of Pan-African metamorphism.

6.2. Resetting of monazite

Apart from documenting the existence of different stages of the tectonometamorphic evolution of the KKB the investigation of monazites with the electron microprobe provides strong evidence that Lower Proterozoic and Pan-African ages were locally reset to significantly younger values.

It has been inferred from two-feldspar thermometry that peak metamorphic temperatures in the KKB during Pan-African orogeny most likely were significantly higher than previously assumed and reached ~ 900°C (Braun et al., 1996). The application of Al-in-Opx thermometry to selected KKB rocks by Chacko et al. (1996) gave further support to this suggestion and pointed to even higher temperatures of ~ 1000°C. If the closure temperature of the Th–U–Pb system in monazite is about 750°C as suggested by several authors (Copeland et al., 1988; Machado et al., 1989; Parrish, 1990; Suzuki et al., 1994) it should be expected that temperatures exceeding 900°C were high enough to reset the Th–U–Pb system completely and to wipe out any information older than Pan-African unless the monazites were shielded during the high-temperature event by minerals like garnet, which are rather 'inert' to Pb exchange with monazite (Montel et al., 1995). In contrast to this, a number of monazites we analyzed preserved Lower Proterozoic ages and did not show any chemical or age zonation which could indicate a diffusion process although they were not shielded from Pb loss. Instead, they occurred at grain boundaries, in retrograde reaction zones around garnet and inclusions in garnet or other phases were connected with the matrix by fractures. We therefore suggest that thermal diffusion of Pb was rather ineffective in resetting Lower Proterozoic and/or Pan-African ages. Further, our results indicate that the closure temperature for Pb diffusion in monazite must be significantly higher than 750°C and should be expected to be in the range of closure temperatures for zircon (> 900°C).

The interaction of the studied rocks with hydrothermal fluid phases during retrograde metamorphism is visible particularly in the augen gneiss and to a lesser extent in the other samples and documented by the alteration of feldspars as well as the replacement of ilmenite by sphene. This process occurred very localized along small fractures or at grain boundaries. Concerning the Th–U–Pb system in monazite our data suggest that in zones where fluid-rock interaction took place monazites were also affected. Fig. 5c shows a SEM image of a euhedral monazite grain from the leptynitic gneiss sample K3. The core of this grain displays a complex patchwork-like structure of small domains with strongly varying Th and, to a lesser extent, U abundances. Toward the rim, Th and U concentrations decrease from 10 to 6 wt.% and from 0.73 to 0.61 wt.%, respectively. Pb abundances are relatively high in the core (0.31–0.47 wt.%) and low at the rim. In contrast to this complex element distribution pattern the calculated ages are rather homogeneous and constitute a single Pan-African population. Microscopic investigation in polarized light revealed the existence of a small fracture transecting the grain near its rim (Fig. 5d). A close inspection of this area showed that along the fracture Pb concentrations drop from 0.2 wt.% (no. 33) to 0.14 wt.% and even lower (0.09 wt.%, no. 36) while Th and U abundances remained almost constant. Simultaneously, calculated ages drop

from 509 to 370–380 and 223 Ma (Fig. 5d). Although the existence of Pb core–rim diffusion profiles, which could indicate thermal Pb diffusion, and simultaneously decreasing apparent ages has been documented by Suzuki et al. (1994) our investigations suggest that mobilization of Pb from monazite and a partial or complete resetting of its Th–U–Pb system and corresponding ages mainly occurred due to interaction with a hydrous fluid phase. The distribution of ages in Fig. 5d as well as in other investigated monazites shows that mobilization occurs only within a few micrometers away from the monazite-fluid interface. Our results are in line with the experimental investigations of Poitrasson et al. (1996) and Teufel and Heinrich (1997) which also emphasized the importance of hydrothermal activity in affecting the Th–U–Pb system of monazite. We therefore conclude that during regional metamorphism even at high temperatures ($< 900°C$) monazite should hardly be affected by thermal Pb diffusion. Considerable change of its Th–U–Pb system in this temperature regime, however, should be expected if fluid-rock interaction took place.

With regard to the geological evolution of the KKB age, resetting in the gneisses most likely occurred contemporaneous to the emplacement of granitic pegmatites subsequent to the peak of Pan-African metamorphism. This is corroborated by the overlap of calculated mean ages from the pegmatites (460–500 Ma) with the presence of an Ordovician age population in the leptynitic gneiss (K3) and the augen gneiss sample (K18). It is suggested that the pegmatitic melts were rich in fluid phases which during crystallization were released and migrated into the adjacent gneisses along localized pathways where they caused alteration of feldspars and ilmenite as well as mobilization of Pb in monazite. The influence of hydrothermal activity subsequent to Pan-African high-grade metamorphism has also been recognized in the Precambrian basement of southern Madagascar by Nicollet et al. (1995). Here, samples within major shear zones display a resetting of Pan-African ages to significantly lower values (375–480 Ma). According to the authors resetting was due to hydrothermal fluids mobilized during the uplift of the Precambrian basement along the shear zones which themselves acted as pathways for a channelized fluid flow.

Acknowledgements

This work was performed during a research stay of I. Braun at the Department de Géologie, Université Blaise Pascal, Clermont-Ferrand/France, funded by the French Government ('Bourse de gouvernement français') and the 'Deutscher Akademischer Austauschdienst (DAAD)'. We like to thank M. Veschambre for providing the microprobe facilities. The constructive reviews by J.-P. Respaut and N.B.W. Harris helped to improve the manuscript and are greatly acknowledged.

References

.

Berger, M., Braun, I., 1997. Pb–Pb dating of apatite by stepwise dissolution technique. Chem Geol. 142, 23–40.

Brandon, A.D., Meen, J.K., 1995. Nd isotopic evidence for the position of southernmost Indian terranes within East Gondwana. Prec. Res. 70, 269–280.

Braun, I., Raith, M., Ravindra Kumar, G.R., 1996. Dehydration-melting phenomena in leptynitic gneisses and the generation of leucogranites: a case study from the Kerala Khondalite Belt, southern India. J. Petrol. 37, 1285–1305.

Chacko, T., Ravindra Kumar, G.R., Newton, R.C., 1987. Metamorphic P–T conditions of the Kerala (South India) Khondalite Belt: a granulite facies supracrustal terrain. J. Geol. 96, 343–358.

Chacko, T., Ravindra Kumar, G.R., Meen, J.K., Rogers, J.J., 1992. Geochemistry of high-grade supracrustal rocks from the Kerala Khondalite Belt and adjacent massif charnockites, south India. Prec. Res. 55, 469–489.

Chacko, T., Lamb, M., Farquhar, J., 1996. Ultra-high temperature metamorphism in the Kerala Khondalite Belt. In: Santosh, M., Yoshida, M. (Eds.), The Archaean and Proterozoic Terrains in southern India within East Gondwana. Gondwana Research Group Memoir—3, pp. 157–165.

Choudhary, A.K., Harris, N.B.W., Van Calsteren, P., Hawkesworth, C.J., 1992. Pan-African charnockite formation in Kerala, south India. Geol. Mag. 129, 257–264.

Cocherie, A., Legendre, O., Peucat, J.J., Kouamelan, A., 1997. In-situ Th–U–Pb dating using an electron microprobe: a powerful tool for complex polygenic monazites. Terra Abst. 9, 441.

Copeland, P., Parrish, R.R., Harrison, T.M., 1988. Identification of inherited radiogenic Pb in monazite and its implications for U–Pb systematics. Nature 333, 760–763.

Fuhrman, M.L., Lindsley, D.H., 1988. Ternary-feldspar modeling and thermometry. Am. Mineral. 73, 201–215.

Harris, N.B.W., Santosh, M., Taylor, P.N., 1994. Crustal evolution in south India: Constraints from Nd isotopes. J. Geol. 102, 139–150.

Hölzl, S., Köhler, H., Kröner, A., Jaeckel, P., Liew, T.C., 1991. Geochronology of the Sri Lankan basement. In: Kröner, A.

(Ed.), The Crystalline Crust of Sri Lanka: Part I. Summary of Research of the German–Sri Lankan Consortium. Geological Survey Department of Sri Lanka Professional Paper 5, pp. 237–257.

Hölzl, S., Hofmann, A.W., Todt, W., Köhler, H., 1994. U–Pb geochronology of the Sri Lanka basement. In: Raith, M., Hoernes, S. (Eds.), Tectonic, Metamorphic and Isotopic Evolution of Deep Crustal Rocks, with Special Emphasis on Sri Lanka, Prec. Res. 66, pp. 123–149.

Kroll, H., Evangelakakis, C., Voll, G., 1993. Two-feldspar geothermometry: a review and revision for slowly cooled rocks. Contrib. Mineral. Petrol. 114, 510–518.

Machado, N., Goulet, N., Gari'py, C., 1989. U–Pb geochronology of reactivated Archean basement and of Hudsonian metamorphism in the northern Labrador Trough. Can. J. Earth Sci. 26, 1–15.

Montel, J.-M., Veschambre, M., Nicollet, C., 1994. Datation de la monazite à la microsonde électronique. C.R. Acad. Sci. Paris 318, 127–146.

Montel, J.-M., Foret, S., Veschambre, M., Nicollet, C., Provost, A., 1996. A fast, non-expensive, reliable, in situ dating technique: Electron microprobe ages on monazite. Chem. Geol. 131, 37–53.

Nicollet, C., 1990. Crustal evolution of the granulites of Madagascar. In: Vielzeuf, D., Vidal, P. (Eds.), Granulites and Crustal Evolution. Kluwer Academic Publishers, Dordrecht. NATO ASI Series C 311, pp. 291–310.

Paquette, J.-L., Nédélec, A., Moine, B., Rakotondrazafy, M., 1994. U–Pb, single zircon Pb-evaporation and Sm–Nd isotopic study of a granulitic domain in SE Madagascar. J. Geol. 102, 523–538.

Parrish, R.R., 1990. U–Pb dating of monazite and its application to geological problems. Can. J. Earth Sci. 27, 1431–1450.

Poitrasson, F., Chenery, S., Bland, D.J., 1996. Contrasted monazite alteration mechanisms and their geochemical implications. Earth Planet. Sci. Lett. 145, 79–96.

Rhede, D., Wendt, I., Förtser, H.-J., 1996. A three-dimensional method for calculating independent chemical U/Pb and Th/Pb-ages of accessory minerals. Chem. Geol. 130, 247–253.

Soman, K., Nair, N.G.K., Golubyev, V.N., Arakelyan, M.M., 1982. Age data on pegmatites of south Kerala and their tectonic significance. J. Geol. Soc. India 23, 458–462.

Srikantappa, C., Raith, M., Spiering, B., 1985. Progressive charnockitization of a leptynite–khondalite suitein southern Kerala, India: evidence for formation of charnockites through a decrease in fluid pressure?. J. Geol. Soc. India 26, 62–83.

Suzuki, K., Adachi, K., 1991. Precambrian provenance and Silurian metamorphism of the Tsunosawa paragneiss in the South Kitakami terrane, Northeast Japan, revealed by the chemical Th–U-total Pb-isochron ages of monazite, zircon and xenotime. Geochem. J. 25, 357–376.

Suzuki, K., Adachi, M., 1994. Middle Precambrian detrital monazite and zircon from the Hida gneiss on Oki-Dogo island, Japan: their origin and implications for the correlation of basement gneiss of Southwest Japan and Korea. Tectonophysics 235, 277–292.

Suzuki, K., Adachi, M., Kazjizuka, I., 1994. Electron microprobe observations of Pb diffusion in metamorphosed detrital monazites. Earth Planet. Sci. Lett. 128, 391–405.

Teufel, S., Heinrich, W., 1997. Partial resetting of the U–Pb isotope system in monazite through hydrothermal experiments: an SEM and U–Pb study. Chem. Geol. 137, 273–281.

Windley, B.F., Razafiniparany, A., Razakamanana, T., Ackermand, D., 1994. The tectonic framework of the Precambrian of Madagascar and its Gondwana connections: a review and reappraisal. Geol. Rundschau 83, 642–659.